

Chapter III:

Water Vapor Uptake in Photolithographic Polymers Observed by Infrared Near-field Scanning Optical Microscopy in a Controlled Environment

3.1 Introduction

Transmission near-field scanning optical microscopy (NSOM) uses a sub-wavelength aperture probe that is scanned in close proximity to the surface of a sample to overcome the diffraction limit on spatial resolution. Infrared-NSOM (IR-NSOM) provides the possibility of vibrational spectroscopy and band specificity with this high spatial resolution. Although visible light is more frequently used with NSOM, IR-NSOM has been used to study systems from semiconductors to polymers to human cells.¹⁻¹¹ This work further develops the IR-NSOM by integrating it into a controlled environment chamber so that samples can be explored in select vapor environments. Previous work with a visible NSOM in vacuum explored the effect of varying temperatures on semiconductor samples.^{12,13} Now, additionally, samples can be exposed to various gases, and the changes they undergo can be monitored.¹⁴

An infrared NSOM has been developed in our group to study chemically amplified photoresists.¹¹ The method has been successful in probing the photoresists spatially and chemically. Chemical subgroup specificity allows for determining the locations of regions of various chemical compounds in polymer films with high spatial resolution. Figure 3.1 shows images of a patterned photoresist consisting of stripes of poly(*t*-butylmethacrylate) (PTBMA) and poly(methacrylic acid) (PMAA). Infrared optical transmission images were taken at 2 different wavelengths with a

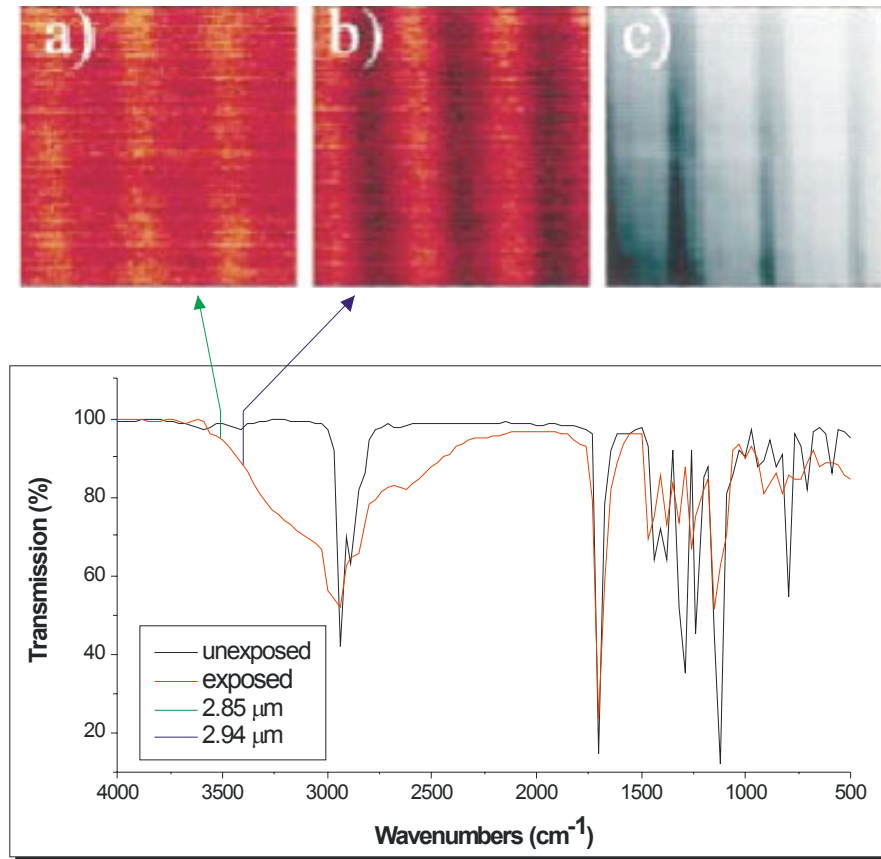


Figure 3.1: Infrared near-field and topographic images (upper panels, 12.5 μm x 12.5 μm) of deep ultraviolet patterned and post-exposure baked poly(t-butylmethacrylate) (PTBMA), and corresponding spectral changes (lower panel) as acquired by an FTIR on non-patterned exposed and unexposed samples. The chemical specificity of the set-up is demonstrated by the difference in contrast when using (a) 2.85 μm wavelength or (b) 2.94 μm. Topographic changes visible in the shear-force image (c) occur due to shrinkage of the exposed areas of the film.

corresponding topographic image. The image in figure 3.1a¹¹ was measured at 2.85 μm , a wavelength at which there is very little absorption by either the modified or unmodified polymer. In a separate experiment, the image in figure 3.1b was measured at 2.94 μm . At this wavelength there is absorption by the exposed polymer, but not by the unexposed. Therefore, there is more contrast in figure 3.1b, indicating the differences in the exposed and unexposed regions of the photoresist. The change in contrast from one IR image to another ($\sim 2\%$) corresponds to the expected absorption contribution from the hydroxyl groups of PMAA. Refractive index contributions to the optical contrast are minimized with narrow field of view collection optics, but still produce a small effect. The success of this IR-NSOM led to the development of the microscope in an environmental chamber described in Chapter II.

Here we study how polymer samples react when exposed to water vapor. This topic has importance for many polymer industries, including packaging, chemical sensors, drug delivery, artificial organs, and electronics. It is particularly important in patterned chemically amplified photoresists, which are used in the fabrication of micro and nanocircuits in the electronics industry.^{15,16} Many polymers swell and change shape when they absorb enough water vapor. The degree of vapor uptake and swelling depends on factors such as film processing and quality, polymer composition and density, molecular orientation of the chains, size and density of pores, and film thickness.¹⁷⁻²¹ Because photochemically modified areas have a different affinity for water than the unexposed areas, swelling of the polymer can cause distortions of

patterns. This can lead to problems with reproducibility and transfer of the desired mask for subsequent etching.

Until now, some of the better methods used to study vapor uptake in polymer films were Fourier transform infrared spectroscopy^{17,22-24} and gravimetric analysis.¹⁸⁻²¹ However, these methods do not provide the spatial resolution that IR-NSOM can; 300 nm spatial resolution has been achieved with transmission IR-NSOM at a wavelength of 3 μm .⁹⁻¹¹ This paper describes the results of an IR-NSOM implemented in a controlled environment chamber to measure vapor uptake and swelling in polymers on a small spatial scale.

3.2 Experimental Materials

Samples used are patterned, acid catalyzed, photolithographic polymers similar to those studied by Dragnea et al.⁹⁻¹¹ A 1.0 μm thick poly(t-butylmethacrylate) (PTBMA) film containing the photoacid generator triphenylsulfonium hexafluoroantimonate was covered by a quartz/chrome mask and exposed to UV light in the range of 200-300 nm. The film was then baked at 130 °C for 5 minutes to activate the acid-catalyzed thermal deprotection chemistry. In the post-exposure bake, the ester groups are converted to a hydrogen bonded carboxylic acid, poly(methacrylic acid) (PMAA), and the volatile product isobutylene is produced, thus shrinking the film substantially in the UV exposed regions. The resulting pattern used here has alternating 2 μm wide lines of approximately 1 μm thick PTBMA and 0.5 μm thick PMAA.

3.3 Experimental Apparatus

The infrared microscope is a variant based on the IR-NSOM apparatus developed by Dragnea et al.⁹⁻¹¹ It is described in detail in Chapter II. A schematic diagram of the set-up is shown in Figure 2.1. The NSOM was built inside a bell jar environmental chamber capable of obtaining pressures down to 0.10 Torr. A Kr⁺ laser pumps a color-center laser, giving 2.6-3.2 μm infrared light, which is absorbed by the O-H stretching vibration of water vapor. For experiments described here, the laser was tuned to a wavelength of 2.85 μm . Figure 3.2 shows that this is a wavelength at which there is low absorption by either the exposed (PMAA) or unexposed (PTBMA) polymer. There should be very little contrast due to the difference in absorbance by these two polymers in the infrared images. However, water is strongly absorbed at 2.85 μm . Therefore, contrast in the optical transmission image can be used to determine regions of the polymer sample with greater amounts of sorbed water. A “map” of the water sorption can be created.

The beam of infrared light enters the bell jar through a CaF₂ window in the chamber’s base plate. The light is coupled into an infrared fiber composed of zirconium aluminum fluoride, which is transparent from 0.45 – 5.0 μm . The fiber is pulled into a tip at one end using a variable-pulling method.^{9,10} The tip is coated with aluminum, typically leaving a 200 nm aperture. Due to the brittleness of the material, some of the tips used in this work may have fractured to sizes larger than 200 nm. The tip is suspended above the sample, which sits on an x-y scanning stage moved by three piezoceramic tube legs. Directly below the sample is a large area, room

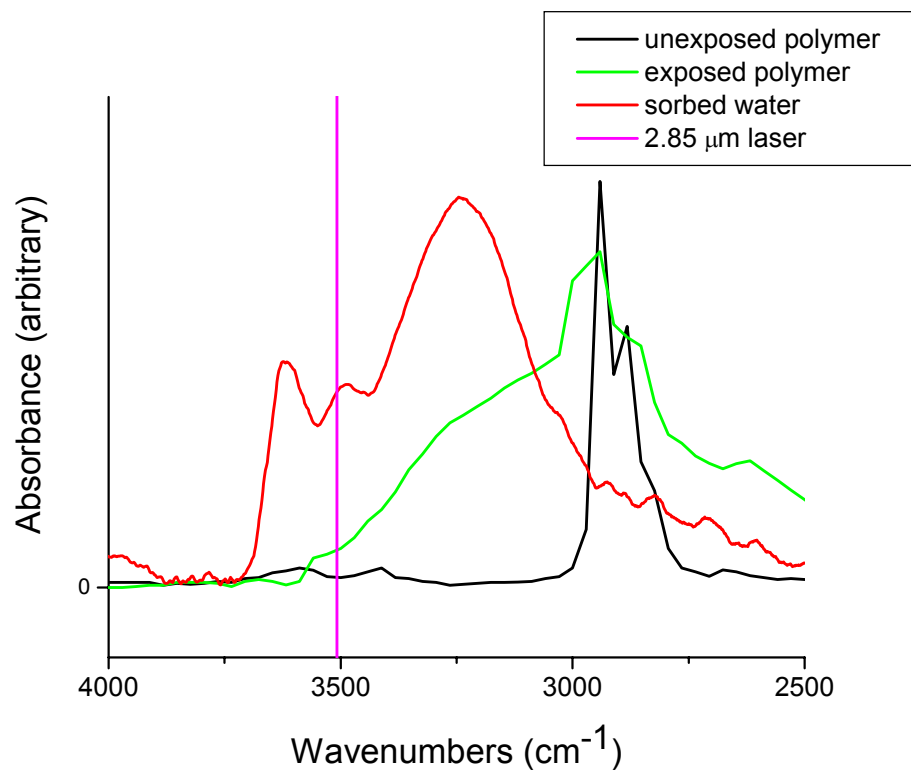


Figure 3.2: FTIR spectra of unexposed polymer (black), exposed polymer (green), water absorbed by the exposed polymer (red); and a line denoting the wavenumber to which the FCL laser is tuned for the IR-NSOM experiment.

temperature, PbS detector, which measures the transmission of the infrared light. The fiber tip is glued to a small tuning fork, which allows the topography to be measured via the shear-force feedback method.²⁵ The scanning and data acquisition are controlled by a scanning probe microscope controller.

All the necessary alignment procedures are carried out before the chamber is evacuated. The IR beam is coupled into the fiber and the tip is positioned above the sample in the near-field. Once the alignment is established, the glass bell-jar is placed on the base plate and the chamber is pumped down. A picomotor screw allows for external control of the tip-sample distance in the z direction when the NSOM is enclosed. Up to 18 Torr of water vapor can be introduced to the chamber and is allowed to equilibrate for at least 45 minutes before a scan begins. In future work, real time measurements of uptake may be possible. Evident problems are the need to follow the changes in distances due to the polymer swelling and to adjust for changes in shear force feedback signals due to the water vapor environment.

3.4 Experimental Procedures

Images shown here are produced by scanning a line 256 times in the x direction, while disabling the scanning in the y direction. Each line scan also consists of 256 points. The transmission of light through the sample and the height of the tip above the sample are simultaneously recorded. The lines can be averaged and plotted to obtain a profile of the topography and transmission of the sample. The averaging produces an improvement in the signal-to-noise ratio. This work shows two sets of

measurements that compare the topography and optical properties of the sample in vacuum conditions and in a water vapor environment.

3.5 Two Micron Features

Topographic images of the sample are shown in Figure 3.3. Figure 3.3a was recorded in a vacuum of 0.10 Torr pressure, while Figure 3.3b was measured in 16 Torr water vapor. Their average line profiles are plotted together in Figure 3.4a to show that when exposed to a water vapor environment the gap between the highest point in the topography image and the lowest point is diminished. Figure 3.4a shows that the depth of the topographical valley is 0.4 μm in vacuum; however, it is actually deeper. Because the fiber tip is too wide, the tip cannot reach the bottom of the valley. Therefore, it cannot produce an accurately scaled topographic image. We know from atomic force microscopy (AFM) experiments done on the sample that the valley is actually 0.5 μm deep. Note also that the region containing PTBMA, the thicker polymer, is not flat. This structure is discussed in detail in previous work,¹¹ and it may be due to some combination of UV irradiation, edge enhancement and shrinkage. A schematic diagram of how the tip might follow the sample's topography is shown in Figure 3.4b.

Figure 3.4a shows that the depth of the valley for the sample exposed to water vapor is only 220 nm. This indicates that the PMAA swells 280 nm more than PTBMA when exposed to 16 Torr water vapor. It is possible that the PTBMA also swells slightly, but we can only measure the relative change. The measured swelling suggests that the PMAA has absorbed more water than the PTBMA.

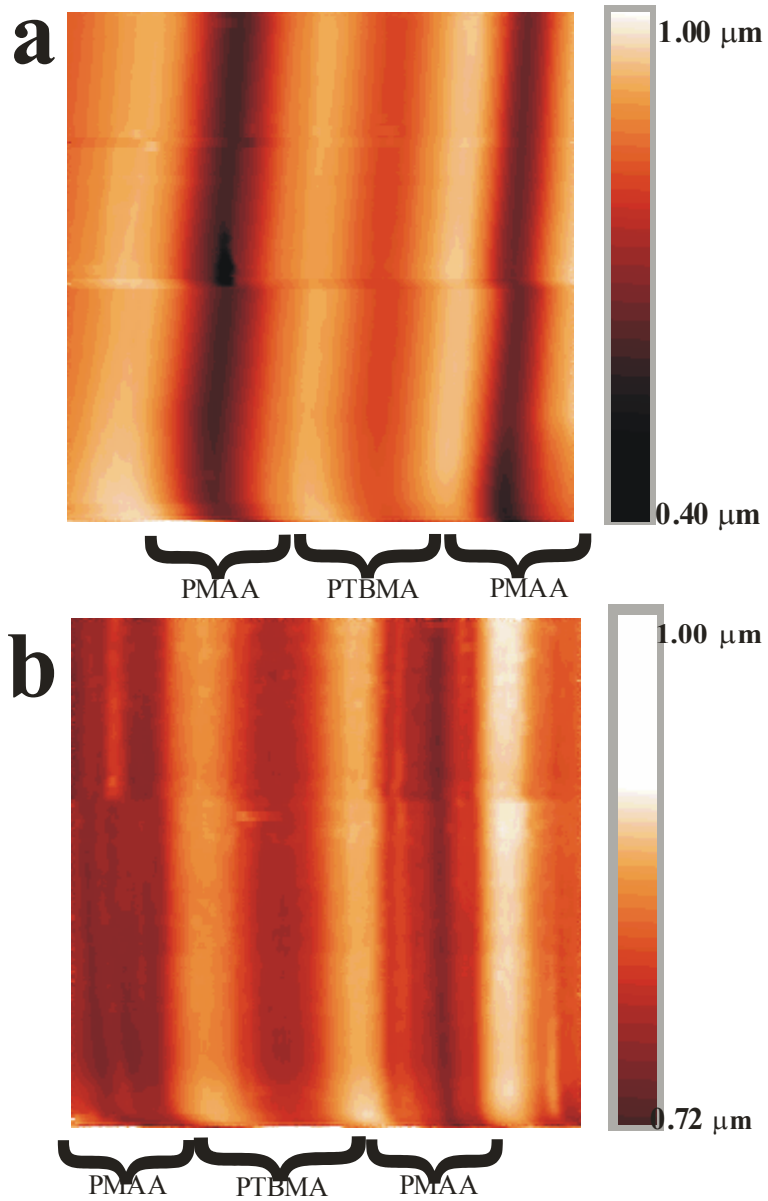


Figure 3.3: Topographic images of photolithographic polymers with 2 μm wide lines. Each image represents a single line scanned 256 times. (a) Topographic linescan of sample in vacuum. (b) Topographic linescan of sample in 16 Torr water vapor environment.

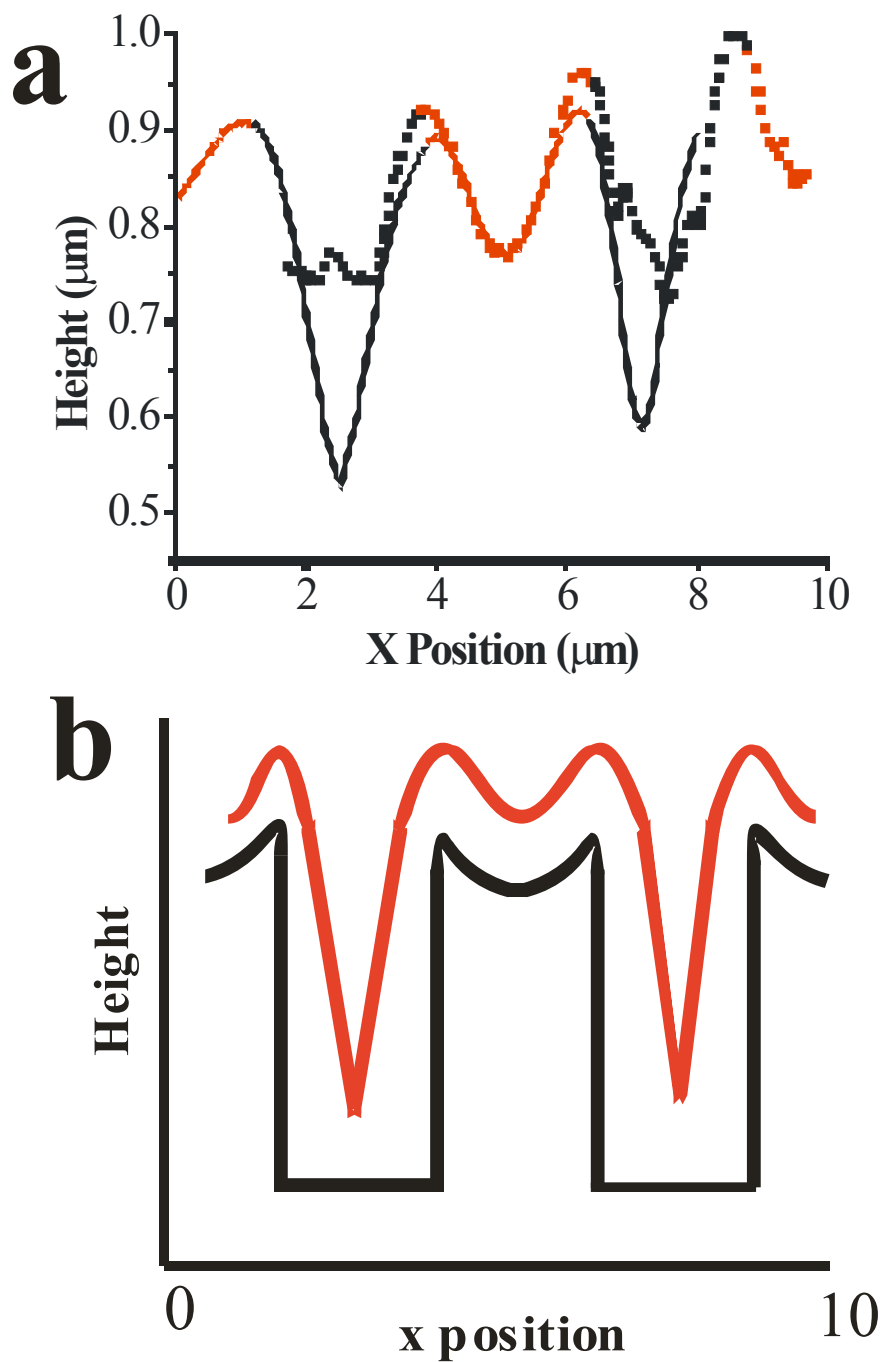


Figure 3.4: (a) Average line profiles. The solid line is an average profile of Figure 3.3a and the dashed line is an average profile of Figure 3.3b. The red line portions represent PTBMA and the black lines represent PMAA. (b) A schematic drawing of the tip following the sample surface. The black line is a profile of the sample's topography, and the red line shows how the tip follows that surface to produce the topography image.

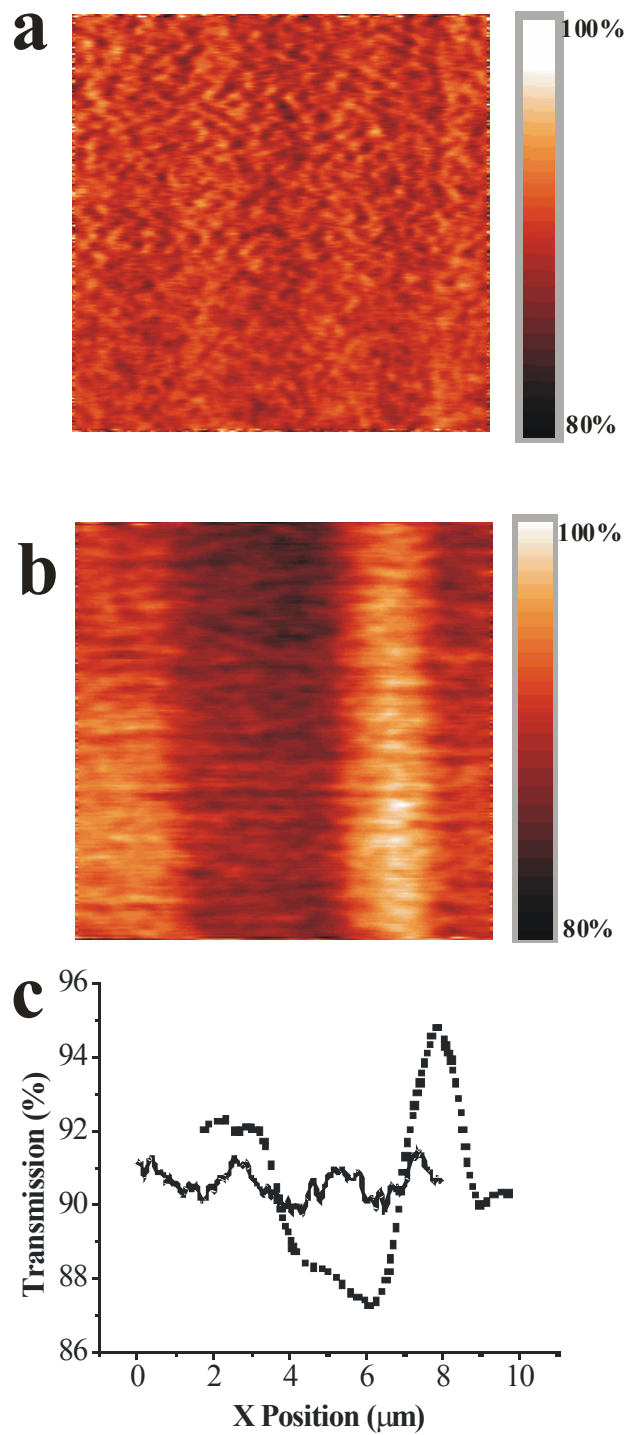


Figure 3.5: Transmission images of 2.85 μm light through photolithographic polymers with 2 μm wide lines. Each image represents a single line scanned 256 times. (a) Transmission linescan recorded in vacuum conditions. Darker regions represent smaller transmission intensity. (b) Transmission linescan recorded in 16 Torr water vapor environment. (c) Average line profiles of parts a and b. The solid line represents the average of the image in part a, the dashed line represents the average of b.

Figures 3.5a and 3.5b show the infrared transmission images recorded simultaneously with the topography images in Figures 3.3a and 3.3b, respectively. Figure 3.5a, recorded under vacuum conditions, shows an image that is almost completely featureless, while Figure 3.5b shows large oscillations in the intensity of light reaching the detector. The reason is that one polymer absorbs more water than the other, thus allowing through less light. Again, the lines were averaged and profiles of these images are plotted in Figure 3.5c. This graph shows a $6 \pm 1\%$ difference between the greatest and the smallest detected intensities. This number was obtained by taking the average of the two local maxima, subtracting the average of the two local minima, then computing error bars using their standard deviations. It is obvious that this contrast is not due to a topographic artifact, since the transmission contrast increases while the topographic contrast decreases. However, the difference is not pure absorption contrast. There are several other contributing factors, which are discussed below.

The modified and unmodified polymers have different indices of refraction. This effect is explained by Dragnea et al.⁹ as a change in cone angle of detection for our particular set-up, and it is expected to produce a variation of 0.5%. It is this effect that causes a slight oscillation of the transmission signal in the vacuum case. Another contrast mechanism can be the change in index of refraction with concentration of water. During vapor uptake, a polymer's index will first increase as void-spaces are filled, and then the index can decrease as the film swells.²⁶ The changes in index of refraction will cause a further change in the amount of light transmitted to the PbS

detector. Depending on the concentration of water in the film, this process can either enhance or diminish the transmission contrast.

Figure 3.6 shows an experiment which was carried out in order to demonstrate this process. A broken tip with an aperture on the order of a few microns is suspended over the sample at a distance which is out of range of the near-field. Therefore, the size of the spot of light that hits the sample is fairly large. The light travels through both modified and unmodified regions of the photoresist before reaching the PbS detector. Under vacuum, the transmission of light through the sample is around 63-64%. Water is slowly introduced into the chamber. At first, this causes an increase in the transmission of infrared light into the sample. This is the opposite of what would normally be expected, because water absorbs infrared light. The result can be explained by index of refraction changes. The introduction of the water causes the void-spaces in the polymer to be filled, and the polymer's index of refraction increases. This causes light to be bent in a different manner as it travels through the sample, and less is reflected off of the interfaces. Therefore, more light arrives at the detector. As more water is added to the chamber, and thus to the polymer, the film swells and causes a decrease in the index of refraction. Now the light rays are bent in such a way that more is reflected at the interfaces. Coupled with the increase in absorption of infrared light by the water, the effect results in a decrease of transmission of infrared light to the detector.

The OH stretching band of water can also change shape depending on the concentration of water. Several examples are cited in the literature.²²⁻²⁴ Therefore, an increase in transmission at one laser wavelength does not always correlate linearly to

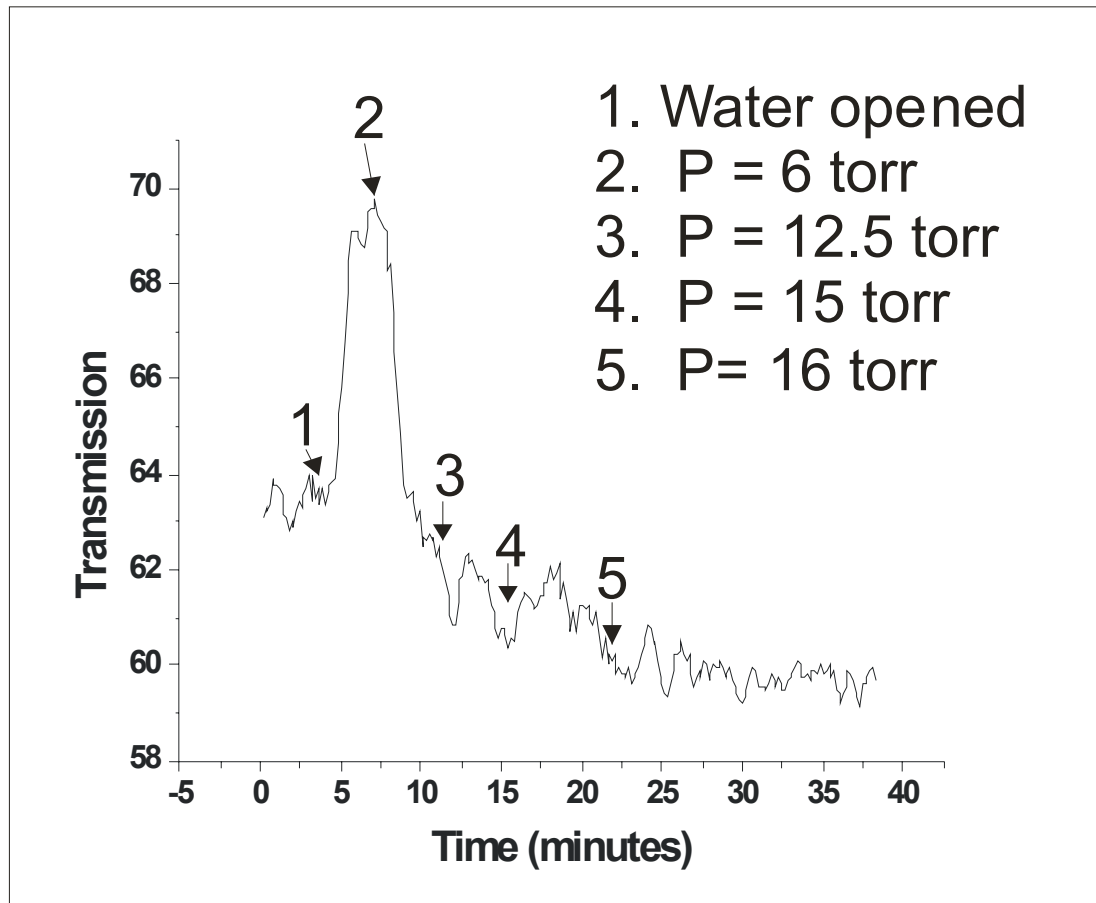


Figure 3.6: Transmission of 2.85 μm laser light through a polymer photoresist sample. The laser is emitting from a large aperture fiber tip and is far from the sample, therefore a large spot size of light hits the sample. A valve is opened slightly to introduce water at a time indicated by the number 1. The partial pressure of water rises slowly and is indicated on the graph until it reaches a pressure of 16 Torr and remains constant.

the amount of water present. This topic will be explored further in Chapter V. In addition, the absorption of light by the gas phase water vapor in the controlled environment chamber will create a baseline that must be subtracted.

Another factor that could decrease the transmission contrast is the size of the NSOM aperture tip. When the tip's aperture is broken or too large, the transmission contrast is not as sharp or as great as it should be.

All of these factors combined make it difficult to determine the concentration of water in the film. In the future, experiments with a quartz crystal microbalance will be performed simultaneously to quantitatively correlate the water concentration in the NSOM signals by more traditional gravimetric methods. Also, use of a tunable laser source with a wider range of available wavelengths will make more experiments accessible. For example, if an image was recorded using a laser tuned to 3750 cm^{-1} , a measurement could be taken that has no contrast contributions from either the OH stretch of the modified polymer or the water. (see Figure 3.2) The percent contrast found in such an image could be subtracted from the contrast in an image measured at 3500 cm^{-1} to minimize index of refraction effects. FTIR experiments should also be carried out to investigate band shifts and give access to information on water molecule interactions.

Optical and topographic images should be spatially consistent. The area that transmits less light should correspond to the region that swells more, because these are the regions with a greater amount of water present. However, in these particular experiments, the optical images are shifted by 2 microns from the topographic images. This is shown in figure 3.7. This is clearly an artifact because similar

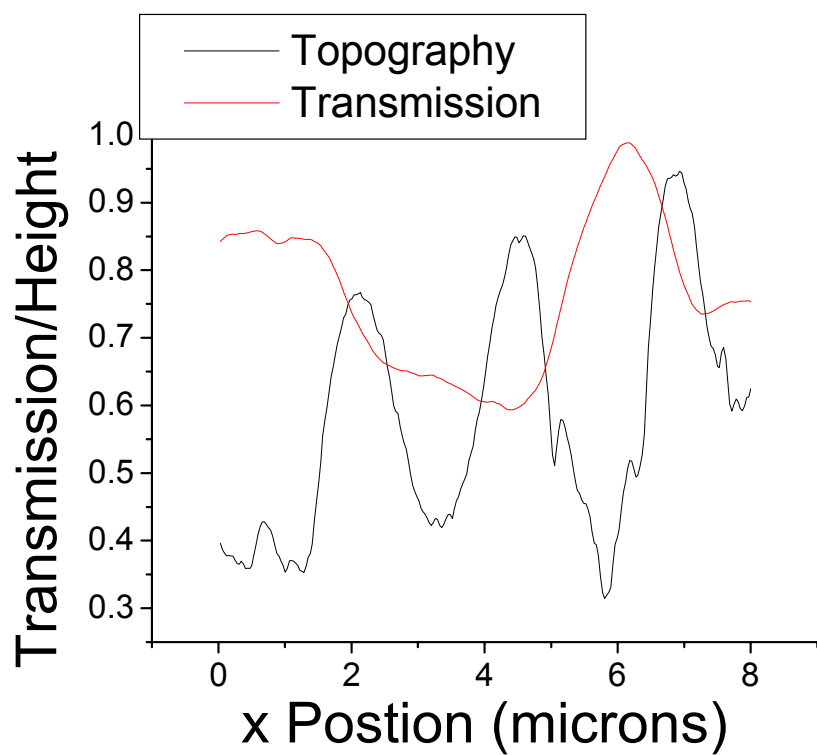


Figure 3.7: Corresponding topography and transmission linescans in a 16 Torr water vapor environment. The topography line (black) is the same as the dotted line shown in Figure 3.4a. The transmission line (red) is the same as the dotted line in Figure 3.5c.

experiments on samples with 4 micron thick lines were also shifted by 2 microns. We do not know why the optical images were shifted but hypothesize that it may be image displacement due to the relatively large probe used. The point on the tip that is interacting with the sample to form the shear force image may be different from the optically transparent region for the transmission intensity. For example, a sharp grain of aluminum coating can protrude from the side of the tip and interact with the sample to form the topographic image, while light emerges from the center of the tip to form the optical image. Future work will correlate the transmission zones with the topographic images more rigorously.

3.6 Four Micron Features

Figure 3.8 shows an example of average linescans on four micron features. The same procedure is carried out as for the above two micron features, but a different area of the sample was probed where four micron features are present. The fiber tip used for these experiments is different from the one used in the previous experiments. This new fiber tip made it possible to better correlate the transmission and topography images. They match up well, with the topographic valleys (PMAA regions) overlapping the areas with lower transmission. This image was measured in an atmosphere of 18 Torr water vapor. The water, which is present in a higher concentration in the PMAA, absorbs the infrared light and decreases the transmission.

The measurements were repeated several times in various environments. The results are summarized in table 3.1. For each environment, we report the depth of the valley (ΔH) and the transmission contrast (ΔT). In an 18 Torr water vapor

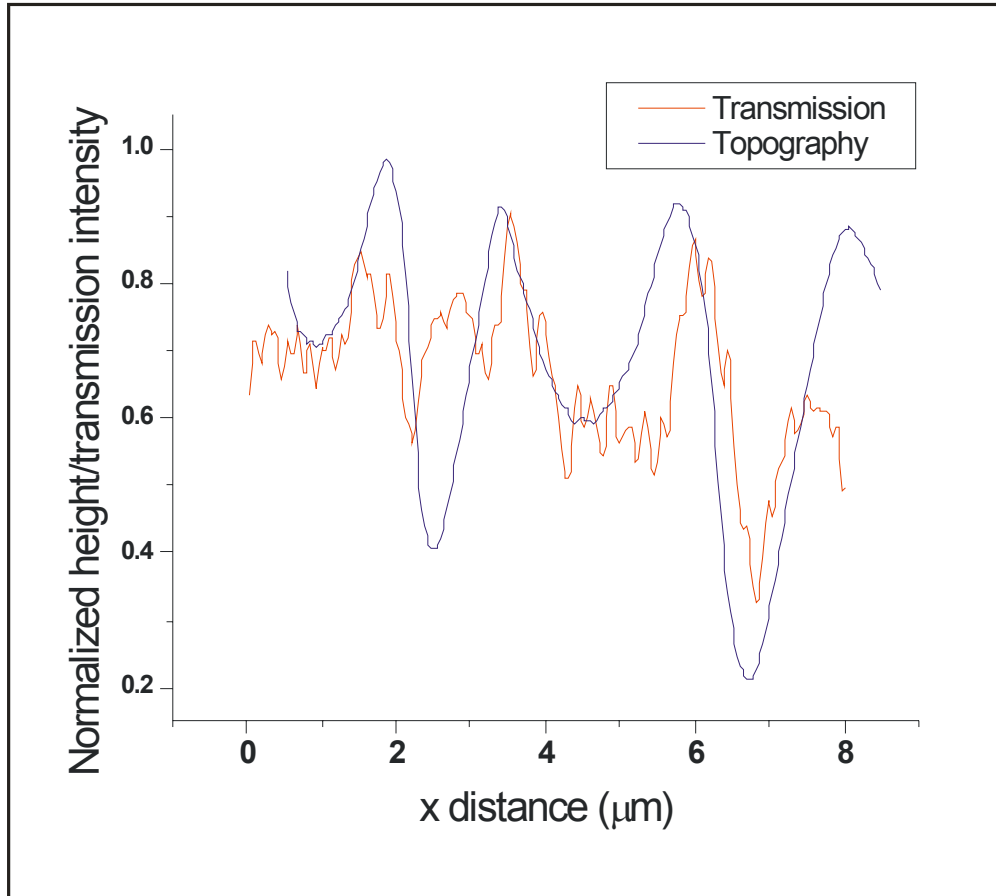


Figure 3.8: Average linescans in transmission and topography for 4 micron features of a polymer photoresist in 18 Torr water vapor.

environment, the PMAA swells 0.20 ± 0.09 microns more than the PTBMA. The error bars were determined by multiple runs with the same tip. This matches well with the result of 0.28 microns swelling found on the 2 micron feature experiments in the above section.

Table 3.1: Height and Transmission data in various experimental conditions

Environment	ΔH (μm)	ΔT (%)
Vacuum (0.20 Torr)	0.56 ± 0.05	$0.35\% \pm 0.02\%$
10 Torr Water Vapor	-	$0.40\% \pm 0.02\%$
18 Torr Water Vapor	0.36 ± 0.04	$0.45\% \pm 0.02\%$

The change in transmission shows that there is a 0.10% difference in transmission contrast in going from a dry to a water vapor environment. This result is quite different from the result on two micron images, which was $6 \pm 1\%$. The difference could be due to differences in the tip used and its aperture. The aperture on the tip used for these experiments could be larger in size, or even slightly broken, thus reducing the contrast. This result highlights the need for consistent tips in order to make comparisons between experiments.

On the positive side, the result also shows the sensitivity of the IR-NSOM. It was able to determine a range of transmission contrast for three different environments (vacuum, 10 Torr, 18 Torr).

3.7 Conclusions

In order to increase the quality of the images and the information obtained from the IR-NSOM described here, several changes to the experimental set-up are required. First, detection should be improved by replacing the large area, room temperature PbS detector with a liquid nitrogen cooled, small area, photovoltaic InSb detector.¹⁰ Use of varying numerical aperture collection optics would assist in reducing the contrast due to the cone angle effect.⁹ Efforts can also be made to facilitate real-time measurements of vapor uptake. One way to achieve this would be to operate in constant height mode, rather than constant gap mode, so that the probe would not interact with the sample. It will also help to determine the source of the changes in the shear-force feedback signals with change in water vapor pressure. Perhaps the use of a non-absorptive glue to stick the fiber on the tuning fork will solve this problem and allow for time-resolved measurements.

This work demonstrates a new method for exploring the vapor uptake of polymers. The shear-force topographic method produces a value for the swelling of a polymer in a vapor environment and, with calibration of a known system, can become a precise measure of the amount of water absorbed in the sample. The transmission data complements the topographic images, and the results can be used to quantify the amount of water in a sample if more work is completed to separate the various contributing effects. Infrared NSOM under environmental control is an excellent potential new tool for determining where water vapor uptake occurs in a polymer sample on a small spatial scale.

References for Chapter III

- (1) Dragnea, B.; Leone, S. R. *Int. Rev. Phys. Chem.* **2001**, *20*, 59.
- (2) Schaller, R. D.; Saykally, R. J. *Langmuir* **2001**, *17*, 2055.
- (3) Stranick, S. J.; Chase, B.; Michaels, C. A. *Abstracts of ACS* **2001**, *221*, 173.
- (4) Cricenti, A. *J. Alloys Compds* **2001**, *328*, 2.
- (5) Hong, M. K.; Jeung, A. G.; Dokholyan, N. V.; Smith, T. I.; Schwettman, H. A.; Huie, P.; Erramilli, S. *Nuc. Inst. Mths. Phys. Res.* **1998**, *144*, 246.
- (6) Knoll, B.; Keilmann, F. *Appl. Phys. A* **1998**, *66*, 477.
- (7) Sahlin, J. J.; Peppas, N. A. *J. Appl. Polym. Sci.* **1997**, *63*, 103.
- (8) La Rosa, A. H.; Yakobson, B. I.; Hallen, H. D. *Appl. Phys. Lett.* **1997**, *70*, 1656.
- (9) Dragnea, B.; Preusser, J.; Schade, W.; Leone, S. R.; Hinsberg, W. D. *J. Appl. Phys.* **1999**, *86*, 2795.
- (10) Dragnea, B.; Preusser, J.; Szarko, J. M.; Leone, S. R.; Hinsberg, W. *J. Vac. Sci. Technol. B* **2001**, *19*, 142.
- (11) Dragnea, B.; Preusser, J.; Szarko, J. M.; McDonough, L. A.; Leone, S. R.; Hinsberg, W. *Appl. Surf. Sci.* **2001**, *175-176*, 783.
- (12) Gray, M. H.; Hsu, J. W. P. *Rev. Sci. Inst.* **1999**, *70*, 3355.
- (13) Gray, M. H.; Hsu, J. W. P. *Appl. Phys. Lett.* **2000**, *76*, 1294.
- (14) Elbs, H.; Fukunaga, K.; Stadler, R.; Sauer, G.; Magerle, R.; Krausch, G. *Macromolecules* **1999**, *32*, 1204.
- (15) Padmanaban, M.; Endo, H.; Inoguchi, Y.; Kinoshita, Y.; Kudo, T.; Masuda, S.; Nakajima, Y.; Pawlowski, G. *Proc. SPIE* **1992**, *1672*, 141.

- (16) MacDonald, S. A.; Cleacak, N. J.; Wendt, H. R.; Willson, C. G.; Snyder, C. D.; Knors, C. J.; Deyoe, N. B.; Maltabes, J. G.; Morrow, J. R.; McGuire, A. E.; Holmes, S. J. *Proc. SPIE* **1991**, *1466*, 2.
- (17) Sutandar, P.; Ahn, D. J.; Franses, E. I. *Macromolecules* **1994**, *27*, 7316.
- (18) Buchold, R.; Nakladal, A.; Gerlach, G.; Herold, M.; Gauglitz, G.; Sahre, K.; Eichhorn, K. J. *Thin Solid Films* **1999**, *350*, 178.
- (19) Chen, W. L.; Shull, K. R.; Papatheodorou, T.; Styrkas, D. A.; Keddi, J. L. *Macromolecules* **1999**, *32*, 136.
- (20) Hutcheon, G. A.; Messiou, C.; Wyre, R. M.; Davies, M. C.; Downes, S. *Biomaterials* **2001**, *22*, 667.
- (21) Neogi, P. *Diffusion in Polymers*; Marcel Dekker, Inc.: New York, 1996.
- (22) Ping, Z. H.; Nguyen, Q. T.; Chen, S. M.; Zhou, J. Q.; D., D. Y. *Polymer* **2001**, *42*, 8461.
- (23) Yarwood, J.; Sammon, C.; Mura, C.; Pereira, M. *J. Mol. Liq.* **1999**, *80*, 93.
- (24) Linossier, I.; Gaillard, F.; Romand, M.; Feller, J. F.; Sci., J. A. P. *J. Appl. Polym. Sci.* **1997**, *66*, 2465.
- (25) Karrai, K.; Grober, R. D. *Appl. Phys. Lett.* **1995**, *66*, 1842.
- (26) Cross, G. H.; Ren, Y.; Swann, M. J. *Analyst* **2000**, *125*, 2173.